Temperature-Dependent Performance of Electrospray Thrusters with ASCENT Monopropellant

Temperature-Dependent Performance of Electrospray Thrusters with ASCENT Monopropellant

IEPC-2024-782

Presented at the 38th International Electric Propulsion Conference, Toulouse, France
June 23-28, 2024

Amelia R. Bruno*, Matthew N. Corrado†, and Paulo C. Lozano‡
Massachusetts Institute of Technology, Cambridge, MA 02139, USA

In this work, we investigate the emission characteristics and performance of a passively-fed electrospray thruster with ASCENT (AF-M315E) monopropellant at temperatures from 20C to 60C. The current-voltage characteristics, energy spectra, beam divergence, and mass spectra of the thruster are quantified in both the positive and negative emission modes. Results show that the startup voltage of the thruster decreases as temperature increases. The average specific charge of the ion plume also decreases, more dramatically in the positive mode than the negative mode, but is offset by a decrease in energy efficiency. When incorporating these losses, we find a relatively constant thrust with increased temperature (around 6-7 uN at 100uA and 10-12 uN at 150uA) which is surprising given previous work with conventional ionic liquids. Specific impulse is found to decrease with temperature, from roughly 680 s at 20C to 580 s at 60C. Thrust-to-power is found to increase slightly with temperature due to a decrease in required power.

I. Nomenclature

F	=	thrust, including efficiencies, N
F_{TOF}	=	thrust, estimate from time of flight, N
g	=	acceleration due to gravity, m/s^2
I_{em}	=	emitted current, A
I_{sp}	=	specific impulse, including efficiencies, s
$I_{sp,TOF}$	=	specific impulse, estimate from time-of-flight, s
L_{TOF}	=	time of flight test section length, m
q/m	=	specific charge, C/kg
$\dot{m}$	=	mass flow rate, kg/sec
η_E	=	energy efficiency
η_p	=	polydispersive efficiency
η_T	=	total efficiency
η_ϕ	=	angular efficiency
T	=	temperature, ^{o}C
t_{TOF}	=	flight time, s
V_0	=	emitter firing voltage, V
V_B	=	beam voltage, V
V_{RPA}	=	retarding potential analyzer voltage, V

*Ph.D. Candidate, Department of Aeronautics and Astronautics, arbruno@mit.edu.
†Ph.D. Candidate, Department of Aeronautics and Astronautics, mcorrado@mit.edu.
‡M. Alemán-Velasco Professor, Department of Aeronautics and Astronautics, plozano@mit.edu

II. Introduction and Motivation

Small satellites are typically limited to one of two primary modes of propulsion: chemical or electric. The two modes offer complementary performance in terms of thrust and specific impulse. However, conventional chemical and electric systems are highly incompatible in terms of system hardware, propellant type, and operational requirements. This means that to utilize both types of propulsion, a spacecraft would need to carry two completely independent systems with separate propellant and propellant management. While possible on large spacecraft, this is generally difficult on small satellites with heavily constrained mass, volume, and power. This has sparked significant research into architectures and strategies that combine various modes of propulsion into a more compact package.

One of the most promising system architectures is the combination of chemical monopropellant and electrospray thrusters using a shared energetic ionic liquid propellant. In particular, the use of ASCENT (formerly AF-M315E) monopropellant has been proposed for use in a chemical-electrospray system, allowing for near-ideal performance in both modes. A prominent example of this is the planned Green Propulsion Dual-Mode (GPDM) mission, a proposed technology demonstration mission for chemical-electrospray ASCENT propulsion.[1,2] This mission is led by NASA Marshall Space Flight Center and features a 3U bimodal propulsion system payload onboard a 6U CubeSat, targeting a launch no earlier than 2025. The MIT Space Propulsion Laboratory (SPL) is providing the electrospray thrusters for GPDM and as such has investigated the integration and performance of electrospray thrusters with ASCENT in recent years.[3,4] As the mission progresses and the concept of operations becomes defined, it is important to characterize how the thrusters will perform in the thermal environments it will be exposed to in orbit, as well as to determine operational ranges of the thrusters. Recent thermal analysis indicates that the electrospray thrusters on GPDM may see temperatures ranging from -5°C to 60°C based on current mission parameters. Note that this range also considers radiative heating from the nearby chemical monopropellant thruster, a challenge unique to the bimodal system.

It is important to consider these thermal environments during mission planning since temperature is known to affect electrospray performance. While the exact physics of ion emission are complex, the current emitted from an electrospray ion source generally depends on physiochemical properties of its propellant—in particular, the propellant's viscosity, conductivity, and surface tension, all of which vary with temperature.[5–7]

The exact impact of these properties on electrospray thruster performance is best explored experimentally. Early work from Lozano et al.[8] studied ion emission from an externally wetted tungsten emitter and found that current increased at higher temperatures, which they attribute to decreased propellant viscosity and therefore increased fluid flow to the emission site. More recent studies have examined performance of various thruster architectures with EMI-BF_4[9,10] and EMI-Im[11,12] propellants. These studies consistently find that emitted current (and, consequentially, thrust of an electrospray propulsion device) increases with temperature. Corrado[10] documented this behavior specifically in MIT electrospray thrusters and even proposed a method for thrust augmentation via active thermal control.

However, all of this research is confined to conventional ionic liquid (IL) propellants, generally composed of one cation and one anion. ASCENT is a complex mixture of hydroxylammonium nitrate, water, and another highly hygroscopic fuel, essentially making it a multi-part ionic liquid blend.[13,14] Previous work has been done to examine the performance of ASCENT in electrospray thrusters, but is limited to room temperature assessments.[4,15] This work aims to fill this gap by experimentally investigating the performance of a porous electrospray thruster firing ASCENT at the elevated temperatures expected on orbit.

III. Experimental Setup

A. Electrospray Thruster

The thruster used in the GPDM mission, and in this work, is the MIT ion Electrospray Propulsion System (iEPS). The thruster itself is an array of 480 emitter tips laser ablated from a porous glass substrate (Fig. 1a). The substrate is permanently bonded to a MEMS-fabricated silicon frame that features glass posts at its corners to align with and electrically isolate from a gold-plated extractor electrode (Fig. 1b).[16] This comprises the thruster head, which is then mounted atop a propellant tank. The tank assembly holds a small reserve of ionic liquid propellant that is passively fed to the back of the emitter via capillary action. A carbon xerogel distal electrode is embedded in the center of the tank to provide electrical connection to the propellant while mitigating electrochemical reactions.[17]

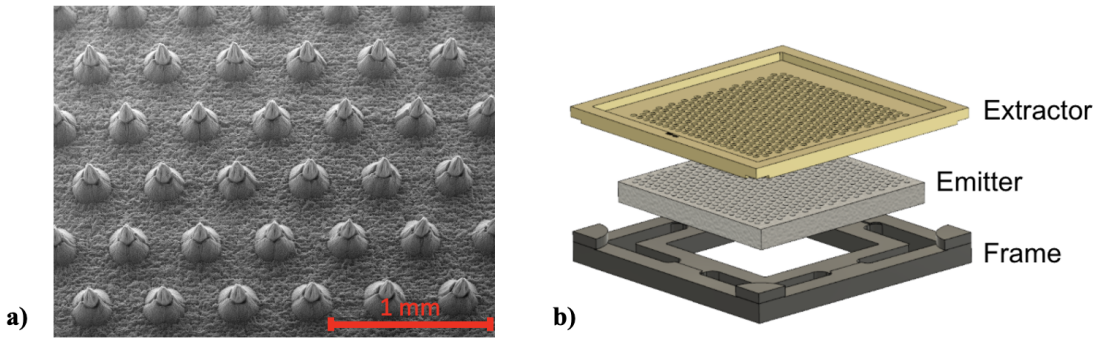

Figure 1: (a) Scanning electron microscope image of emitter tips on an iEPS array. (b) Exploded view of an iEPS thruster head, showing extractor, emitter, and frame.

The standard iEPS design is modified in this work to include an electric heater circuit that can simulate the thermal conditions of interest. The heater circuit consists of three 50 Ω resistors, connected in series and bonded onto three adjacent edges of the silicon emitter frame. A 100 Ω platinum resistance temperature detector (RTD) was bonded to the remaining edge of the frame. This triple-resistor approach was employed due to lessons learned from previous experiments, which found that using fewer resistors at higher output power led to uneven heating and propellant hotspots on the emitter chip during testing.[10] A notional diagram of these elements is shown in Fig. 2a. All components were bonded to the frame using MasterBond Supreme 11AOHT-LO epoxy, which is thermally conductive, electrically insulative, and low outgassing.[18] A suitably thick layer of epoxy between the frame and the heater circuitry was crucial since the frame can be biased to voltages exceeding 1 kV during thruster operation. Additionally, special caution was taken during assembly to ensure no components of the heater circuit bridged the 1 mm gap between the frame and the extractor, which would risk a thruster short. Figure 2b shows a photo of the completed thruster head with heater circuitry mounted onto a propellant tank.

The thruster temperature was controlled using an Arduino-based PID controller, with the RTD temperature input as the process variable and a pulse-width modulation (PWM) signal as the control variable, built by Corrado in previous work.[10] The PWM signal is then fed to a MOSFET switch that controls the voltage to the heater resistors per the prescribed duty cycle. The heater resistors are powered through a 12 V DC power supply, which at a 100% duty cycle has a maximum power output of 0.96 W. After full integration and PID tuning, the temperature measurement and control was found to be accurate to ±1°C at steady state.

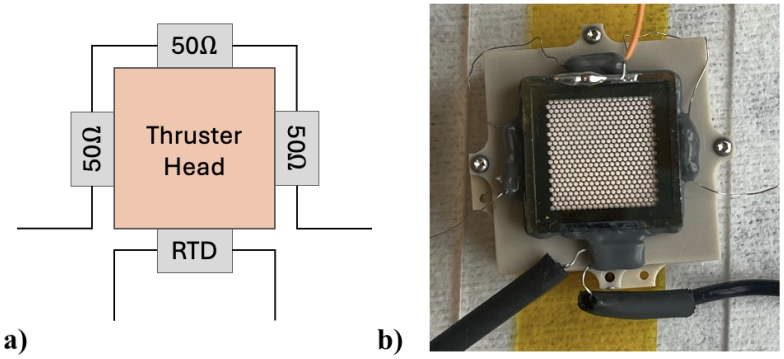

Figure 2: (a) Notional diagram of heater circuit on thruster head. (b) Photo of completed test assembly.

B. Test Environment and Protocols

All tests were conducted in the MIT SPL Turbovac vacuum facility, a ⌀40 x 80 cm chamber with additional mounted extender flange for a custom time-of-flight instrument. The chamber is evacuated by two turbomolecular pumps (68 and 685 L/s) backed by a dry mechanical pump. The chamber base pressure remained below 1E-6 Torr for all tests. For testing, the thruster tank was filled with 0.5 mL of pre-dried ASCENT propellant. The thruster was then installed onto a rotational mount within the Turbovac chamber which could be rotated to direct the plume into different diagnostic instruments.

After the chamber was evacuated to high vacuum, the thruster was started by manually increasing emitter voltage until first emission was observed. The thruster was then conditioned on a alternating-polarity voltage waveform until the emitted current stabilized, approximately 20 min. All performance measurements were taken at temperatures from 20°C to 60°C. The exact measurement setpoints varied by data type: current-voltage (I-V) and time-of-flight (TOF) measurements were taken at intervals of 10°C, while retarding potential analysis (RPA) and beam divergence measurements were taken at intervals of 20°C. The heating rate was ∼1°C/min between setpoints. After reaching a given temperature, the thruster was allowed to dwell for ∼15 min to ensure consistent temperature distribution across the array prior to data collection.

IV. Methodology

A. Current-Voltage Behavior

The thruster is fired by applying a voltage to the emitter, V_0, while the extractor is kept electrically grounded. A Matsusada AS-3B1 high-voltage amplifier was used to supply V_0 with an accuracy of ± 5 V. To characterize the thruster's current-voltage (I-V) behavior, a triangular voltage waveform was applied across the thruster with a 90 s period. The emitted and intercepted currents, defined respectively as the current pulled by the emitter from the lab supply and the current flowing into the extractor, were captured and recorded using custom current-sensing circuitry to within ± 1 µA. To generate I-V curves, the triangular voltage waveform is repeated 8 times, and the resultant currents are recorded and averaged with error propagation considered. Only the falling slope of the voltage waveform is considered in this characterization, since the rising slope includes long periods of low emission, which is not representative of nominal operation.

B. Retarding Potential Analysis

A retarding potential analyzer (RPA) was used to capture the energy spectra of the thruster's plume at each temperature setpoint. The RPA instrument used is based on the design by Lozano[19] and used in previous SPL work.[20,21] The RPA, shown schematically in Fig. 3, consists of a grounded aperture, three high-transparency RPA grids, a second grounded grid, and an electron repelling grid biased to −30 V before a Faraday cup current collector. The RPA grids and the collected current signal are controlled and logged with the same equipment described in Section IV.A. The RPA aperture is ⌀5 mm and positioned approximately 15 cm downstream from the thruster.

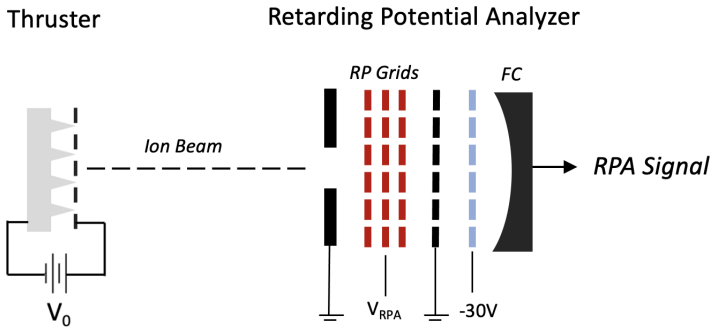

Figure 3: Notional diagram of the retarding potential analyzer used in this work; not to scale.

To collect RPA scans, the thruster was first rotated such that the centerline of the ion plume was aligned with the RPA aperture. The thruster was then fired at a constant voltage while a triangular waveform was applied to the RPA grids, with a maximum value 10% above the magnitude of firing voltage and a minimum value of 100 V in the opposite polarity of the plume. The RPA voltage was swept 8 times at a period of 60 s; note that this necessitates firing for a relatively long duration in a single polarity, which is somewhat unrepresentative of standard operation. In post-processing, the collected current is averaged and normalized with error propagation considered.

C. Beam Divergence

With the retarding potential grids grounded, the RPA instrument shown in Fig. 3 can also be used as a simple Faraday cup collector. This configuration was used to obtain spatial distribution of the ion beam. For these tests, the thruster was fired at a constant current while being manually rotated, so that the plume was swept through a 180-degree arc centered on the RPA aperture. The angular position was recorded with a 2000 step-per-revolution angular encoder (Encoder Products 15T Accu-Coder) and collected current was logged with the same equipment as Section IV.A. The full sweep was repeated 8 times and data was centered, zero-corrected, and averaged in post-processing.

D. Time-of-Flight Mass Spectrometry

The mass spectra of the thruster plume was captured using a custom-built time-of-flight (TOF) mass spectrometer. The TOF instrument works by periodically interuppting the ion beam via an electrostatic deflection gate, approximately 16 cm downstream from the thruster. When the gate is open, the ion species are able to travel through a field-free flight length L_{TOF} until they reach a detector. Assuming all ions are accelerated by the emitter potential V_0, the time for ions to reach the detector t_{TOF} is dependent on their charge-to-mass ratio (q/m) as

$$t_{TOF} = \frac{L_{TOF}}{\sqrt{2\left(\frac{q}{m}\right)V_0}} \tag{1}$$

with $L_{TOF} = 1.11$ m. Figure 4 depicts the instrument. The TOF diagnostic samples a small segment of the ion plume to obtain a high-resolution mass spectra; because of this, the current requires significant amplification. The detector used in this work is a Photonis Magnum 5900 channeltron electron multiplier (CEM) which has a signal gain dependent on its bias voltage. For all tests, the CEM bias voltage was +1.75 kV, which translates to a gain of roughly 10^5. This signal is then further amplified by a factor of 50 through a custom transimpedance amplifier (rise time ≤ 30 ns) and logged on a digital oscilloscope (Keysight DOSX3024A) set to average 2048 traces. In post-processing, the TOF trace is zero-corrected, normalized, and smoothed to obtain the final result.

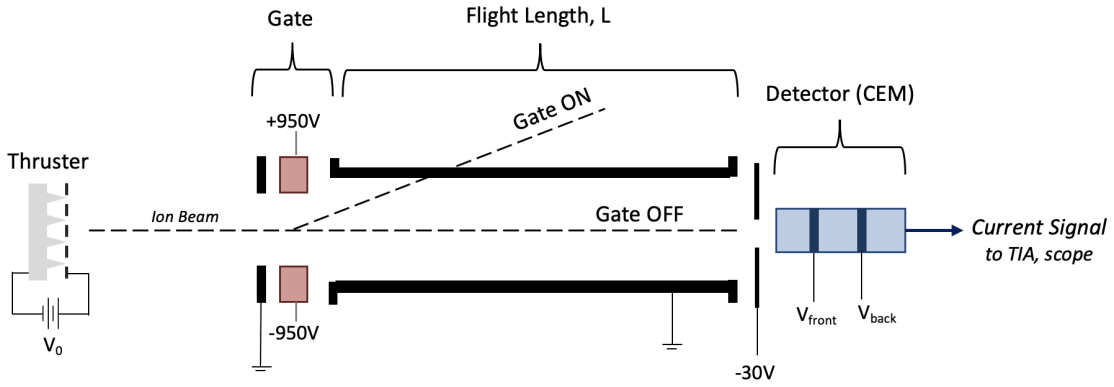

Figure 4: Notional diagram of the time-of-flight instrument used in this work; not to scale. The CEM bias voltage is given by $V_{back} - V_{front}$ and must always be positive to attract the electron cascade.

V. Results

A. Current-Voltage Behavior

Figure 5 shows the I-V curves for the thruster at various temperature setpoints. The data has been separated into positive and negative modes to better view the trends with temperature. While not shown here, the intercepted current remained below 0.5% of the emitted current for all tests. Immediately, we notice an increase in emitted current for the same applied voltage at increased temperature. This agrees with previous work with conventional ILs.[9,10,12] Interestingly, this appears to be caused by both (1) a decrease in the startup voltage with increased temperature, and to a lesser extent, (2) an increase in the slope of the I-V curve with increased temperature. Between the first and final temperature setpoints, the startup voltage decreases by roughly 60 V in both polarities, and the I-V slope increases by 50% or more. Full tabulated values are given in Table 2 in the Appendix. For each +10°C increase, we see a similar jump in I-V performance until ∼50°C, where the curves for 50°C and 60°C begin to collapse together. These trends suggests that the effects on performance may saturate around this temperature, which could be due to a stabilization of the propellant properties.

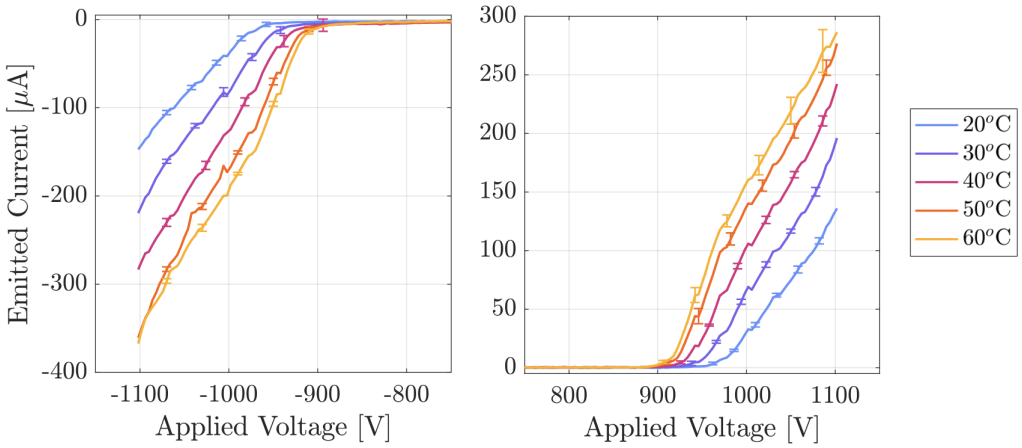

Figure 5: I-V data at various temperatures, negative mode (left) and positive mode (right), with 3σ error bars. Note the difference in y-axis scale between modes.

B. Retarding Potential Analysis

Figure 6 shows RPA scans for the thruster at 20°C, 40°C, and 60°C. It is worth noting that there are no prominent "steps" in the RPA curves that can be easily attributed to known ion fragmentation events, which is generally seen in analyses with conventional ILs. Instead, we observe a beam with some spread of energies between $0.6V_0$ and V_0 in both emission modes. The distribution of energy shifts as temperature increases. This is an unexpected result, as previous studies with conventional ILs generally find no major change in RPA data with temperature,[9,12] although a slight increase in ion fragmentation rate with temperature has be observed in more detailed experiments.[22] Temperature has a more significant effect on beam energy in the positive emission mode; this is likely related to differences in the cation/anion composition of ASCENT, itself an ionic liquid mixture. This increased energy spread has significant impact on thruster performance via energy efficiency. This is discussed further in Section VI.

C. Beam Divergence

Figure 7 shows the spatial beam distribution for the thruster at 20°C, 40°C, and 60°C. We observe little change in the beam's half-angle (encompassing 95% of the beam) with temperature, which stays at about 50° agreeing with previous studies.[9,12] The current distribution appears slightly more Gaussian at higher temperatures, as the 20°C distribution is somewhat asymmetric. One explanation for this is that the increased temperature may promote even wetting across the emitter array, yielding a more consistent current distribution.

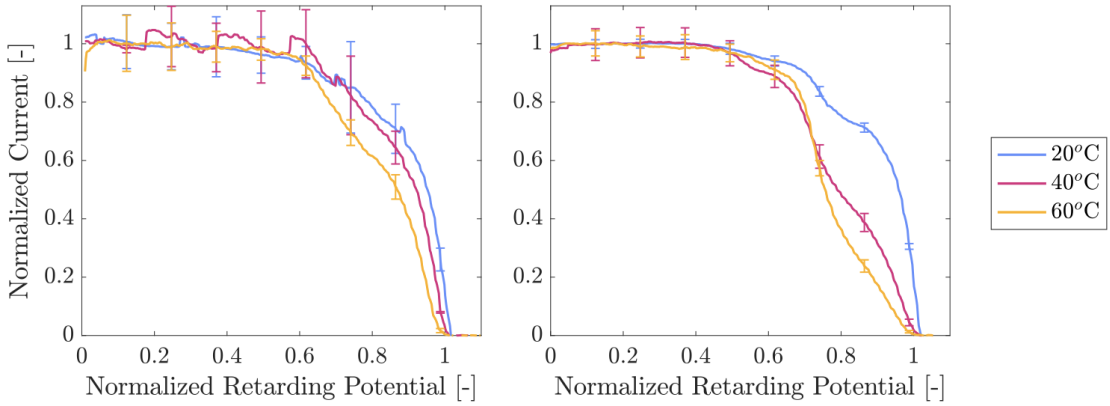

Figure 6: RPA data at various temperatures, negative mode (left) and positive mode (right), $I_{em} = \pm 100\mu A$, with 3σ error bars.

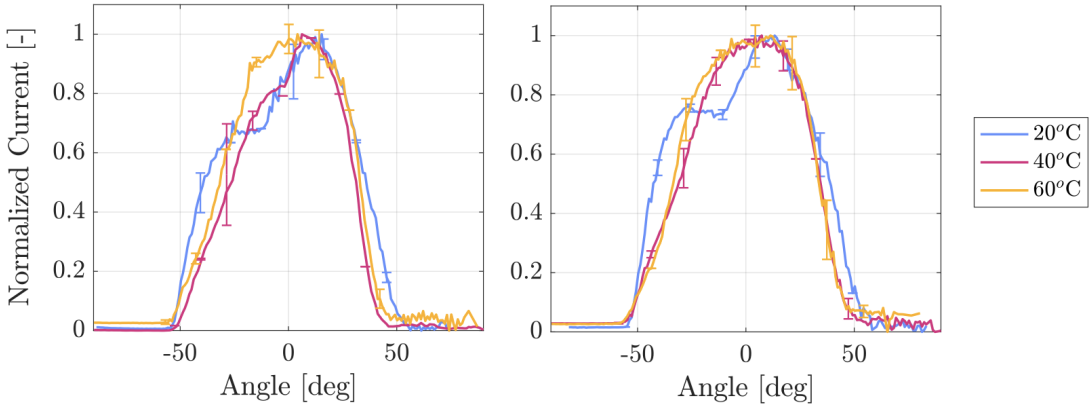

Figure 7: Angular beam distribution at various temperatures, negative mode (left) and positive mode (right), $I_{em} = \pm 100\mu A$, with 3σ error bars.

D. Time-of-Flight Mass Spectrometry

Time-of-flight scans were taken at 20°C to 60°C in increments of 10°C, in both firing polarities, with emission currents of ±100 µA and ±150 µA. The spectra were found to not be dependent on emitted current for the setpoints examined. Fig. 8 shows TOF spectra for ±150 µA at all temperatures. These results show a much larger droplet tail than our previous work.[4] We attribute this to minor upgrades in the TOF procedure, in particular for the biases on the CEM detector. We have recently improved this to more consistently capture signals from the heavy and low-energy species that are unique to ASCENT ion beams and more sensitive to CEM biases.[23] The estimates from this TOF methodology have been supported with direct mass loss measurements, but will be further validated with direct thrust measurements in upcoming work.

The negative mode TOF spectra shows a very consistent composition, where three distinct ion species comprise about 90% of the plume. The remaining 10% is a tail of heavy species or droplets extending out to $\sim 10^4$ amu. The average mass of the negative mode ion beam becomes slightly heavier as temperature increases. The composition of the positive mode ion beam is less consistent: there is a distinct ion step at 76 amu, and then a region of apparent fragmented species, and finally a significant droplet tail out to $\sim 10^4$ amu. The percentage of the beam that is comprised of heavy species or droplets has a strong dependence on temperature. This tail is roughly 20% of the beam at 20°C and increases to nearly 40% of the beam at 60°C. Fig. 9 shows the average specific charge for each TOF scan, illustrating these trends. This has interesting implications for thruster performance that is further discussed in Section VI.

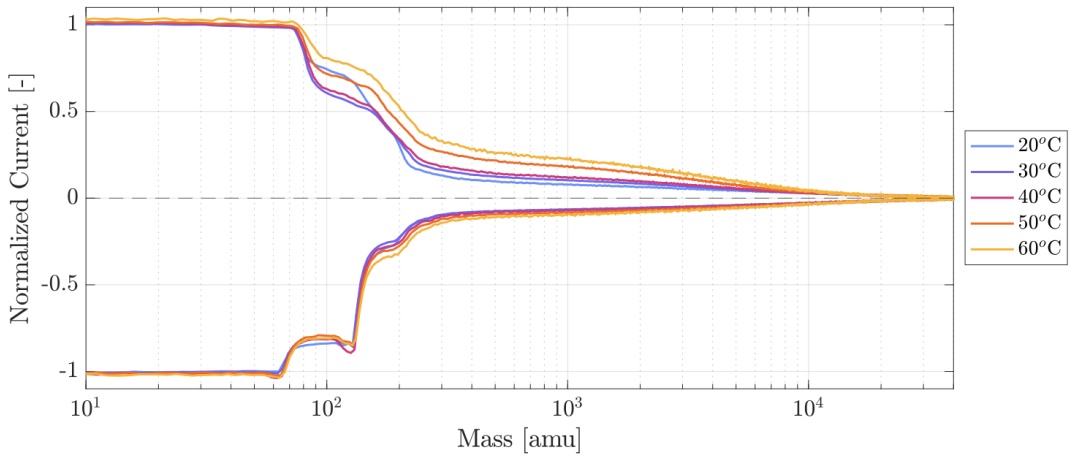

Figure 8: Time-of-flight data at various temperatures, $I_{em} = \pm 150\mu A$. The conversion of the x-axis from flight time to species mass assumes singly-charged ions.

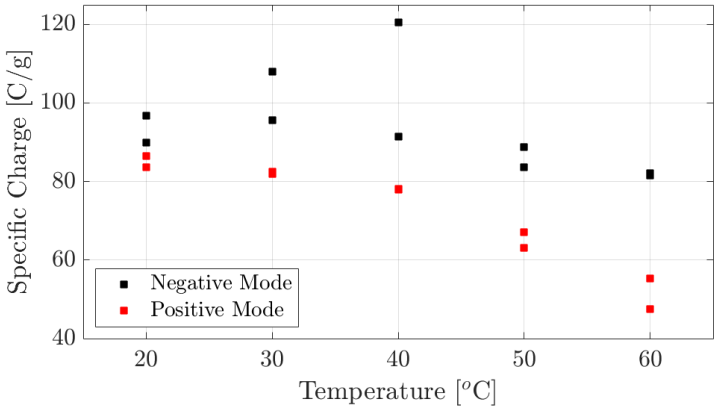

Figure 9: Average specific charge of the ion beam as a function of temperature, various current setpoints.

VI. Discussion and Analysis

A. Analytical Methods

The TOF results can be used to estimate performance of the electrospray thruster. The TOF-inferred thrust, mass flow rate, and specific impulse of the thruster is calculated as:[24]

$$F_{TOF} = \frac{2V_0}{L_{TOF}} \int_0^\infty I_{em} \bar{I}(t) dt \tag{2}$$

$$\dot{m}_{TOF} = \frac{4V_0}{L_{TOF}^2} \int_0^\infty t I_{em} \bar{I}(t) dt \tag{3}$$

$$I_{sp,TOF} = \frac{1}{g} \frac{F_{TOF}}{\dot{m}_{TOF}} \tag{4}$$

where $\bar{I}(t)$ is the normalized current collected by the TOF instrument, as shown in Fig. 8. The TOF-inferred performance results are overestimates of the real performance as they do not include certain losses, such as those from energy inefficiencies and beam spreading. The TOF performance can be corrected using independently obtained efficiency estimates.

The total efficiency of an electrospray thruster, η_T, can be broken into several subcomponents as

$$\eta_T = \eta_i \eta_{tr}^2 \eta_\phi \eta_E \eta_p \tag{5}$$

where η_i is the ionization efficiency, η_{tr} is the transmission efficiency, η_ϕ is the angular (or beam divergence) efficiency, η_E is the energy efficiency, and η_p is the polydispersive efficiency. A detailed discussion of these subcomponents and their derivations can be found in Lozano et al.[8] In this work, we assume that $\eta_i = 1$, i.e. only ionized species leave the thruster. Additionally, since the intercepted current did not exceed 0.5% of the emitted current for all tests, we also assume $\eta_{tr} = 1$. This simplifies Eqn. 12 to $\eta_T = \eta_\phi \eta_E \eta_p$. The remaining efficiency components can be estimated through the thruster measurements presented in previous sections.

The angular efficiency of the thruster captures losses due to spatial spreading of the beam. It can be estimated by integrating the hemisphere of the distribution as:[20]

$$\eta_\phi = \left(\frac{\int_0^{\frac{\pi}{2}} I(\phi) \cos(\phi) \sin(\phi) d\phi}{\int_0^{\frac{\pi}{2}} I(\phi) \sin(\phi) d\phi} \right)^2 \tag{6}$$

where $I(\phi)$ is the current measured by the Faraday cup collector as a function of angle, as shown in Fig. 7.

The energy efficiency accounts for losses in the energy of the ions accelerated by the thruster, and is given by the ratio of the beam potential V_B to the emitter potential V_0. The beam potential is given by the maximum peak of the ion energy spectrum, or the potential corresponding to the maximum slope in the RPA data in Fig. 6. Note that this method does not adequately capture losses due to ion fragmentation, which is included in the polydispersive efficiency.

The polydispersive efficiency of an electrospray thruster captures losses due to ions of varying specific charge being accelerated through and emitted from the thruster. This can be calculated through the TOF-inferred results as:[22]

$$\eta_p = \frac{F_{TOF}^2 / 2\dot{m}_{TOF}}{I_{em} V_0} \tag{7}$$

$$\eta_E = \frac{V_B}{V_0} \tag{8}$$

Finally, the realistic performance of the electrospray thruster can be obtained through a correction factor to the TOF-inferred performance. Note that this factor includes energy efficiency, since experimental results found $\eta_E \not\approx 1$ in some cases, and Eqns. 2-4 use V_0 in their formulations.

$$F = \eta_E \sqrt{\eta_\phi} F_{TOF} \tag{9}$$

$$I_{sp} = \sqrt{\eta_\phi} I_{sp,TOF} \tag{10}$$

$$\eta_T = \eta_i \eta_{tr}^2 \eta_\phi \eta_E \eta_p = \eta_\phi \eta_E \frac{F_{TOF}^2 / 2\dot{m}_{TOF}}{I_{em} V_0} = \frac{F^2 / 2\dot{m}}{I_{em} V_0} \tag{11}$$

$$\eta_\phi \eta_E \frac{F_{TOF}^2}{\dot{m}_{TOF}} = \frac{F^2}{\dot{m}} \tag{12}$$

B. Inferred and Corrected Performance

Table 1 shows the angular, energy, polydispersive, and total efficiencies as a function of temperature in both emission modes. The angular efficiency remains stable around $\eta_\phi \approx 0.7$ across all setpoints. The polydispersive efficiency appears to increase slightly with temperature, more so in the positive mode, but generally remains around $\eta_p \approx 0.3 - 0.45$. These values are considerably less than that of conventional ILs, which typically yield $\eta_p \approx 0.4 - 0.8$ in similar thruster architectures.[20–22] The lower polydispersive efficiency of ASCENT is a direct result of its more complex chemical composition.

A quite surprising result is the change in energy efficiency with temperature in the positive mode. Typically, in thrusters with conventional IL propellant, the energy efficiency can often be approximated at unity and is found to not change with temperature.[21] As shown in Fig. 6, we see a significant change in the average beam energy at higher temperatures, yielding energy efficiencies of $\eta_E^+ = 0.73$ and $\eta_E^+ = 0.71$ at

Table 1: Thruster efficiency results.

Temp.	Mode	η_ϕ	η_E	η_p	η_T
20°C	+	0.70	0.97	0.33	0.22
	-	0.73	0.99	0.30	0.22
40°C	+	0.68	0.73	0.35	0.18
	-	0.75	0.98	0.37	0.27
60°C	+	0.68	0.71	0.44	0.21
	-	0.69	0.95	0.35	0.23

40°C and 60°C, respectively. The combined losses lead to a total thruster efficiency ranging from 18% to 27% across all tests, with no clear trends with temperature.

Figure 10 shows the TOF-inferred thrust at all temperatures, and the corrected thrust for temperatures with complete efficiency data (i.e. for 20°C, 40°C, and 60°C). Data are presented separately for the ±100 µA and ±150 µA emission currents. We see the inferred thrust trend upwards with temperature, more strongly in the positive mode than in the negative mode. However, this is offset by the decrease in energy efficiency. The result is a relatively stable corrected thrust in both modes, around 6-7 µN at ±100 µA and 10-12 µN at ±150 µA. Figure 11 shows the corrected specific impulse and the corrected thrust-to-power. The specific impulse decreases with temperature, in the same trends as the specific charge plotted in Fig. 9, from around 800 s to 600 s after correcting for inefficiencies. Surprisingly, despite thrust remaining fairly constant, we observe a general increase in thrust to power due to the shift in the thruster's I-V curve. At higher temperatures, the thruster produces the same thrust for a given current level, but the voltage required to do so decreases. A full table of performance results is given in the Appendix.

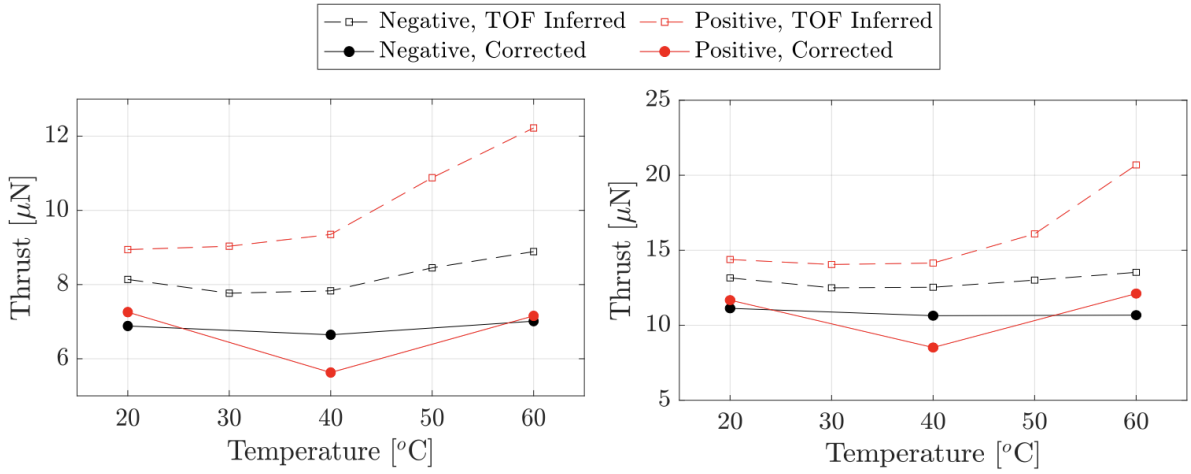

Figure 10: TOF-inferred and corrected thrust as a function of temperature, at (left) $I_{em} = \pm 100$µA and (right) $I_{em} = \pm 150$µA. Note the the difference in y-axis scale between current setpoints.

These findings indicate that temperature impacts the performance of an ASCENT-fueled electrospray through various pathways. The thruster's I-V curve dramatically shifts with temperature, both through a decrease in startup voltage and an increase in I-V slope. The change in startup voltage may be caused by a lower surface tension, which in turn requires a lower electric pressure for Taylor cone formation, or could be caused by the formation of emitting menisci at different locations on the porous tip. The change in the I-V slope can likely be attributed to the lower viscosity of the propellant. The decreased viscosity yields a lower hydraulic impedance in the emitter bulk and therefore a higher mass flow rate. This also enables a "heavier" ion beam as the flow rate becomes much higher than that needed for pure ion emission.[7] The lower specific charge inferred from TOF suggests greater thrust, as found in previous studies.[9,10,12] However, the most

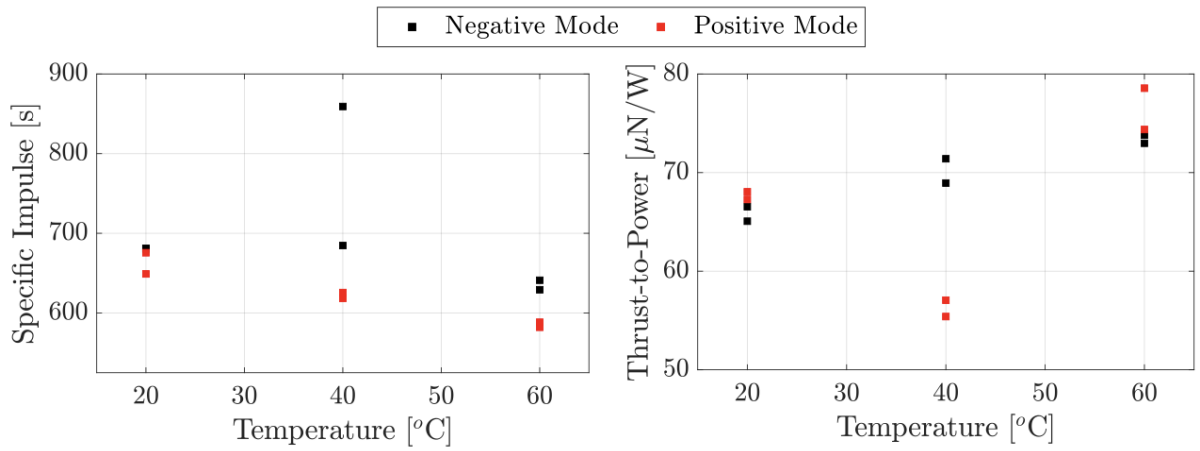

Figure 11: (Left) Corrected specific impulse and (right) corrected thrust-to-power as a function of temperature, various current setpoints.

surprising result of this study is that the increase in thrust from higher mass flow rate is offset by the change in energy of the ion beam. In the positive mode specifically, we observe a 25-30% drop in the average beam energy, or approximately 250 V. We note that this decrease is in line with the typical ohmic loss at the emission site of a cone-jet electrospray.[25,26] This is an interesting observation and suggests that the emission regime of an ASCENT electrospray is highly sensitive to only minor changes to propellant properties. Based on these data, further investigation is recommended to elucidate the exact physics of ASCENT ion emission. A more rigorous experimental approach with a single emitter (rather than an array) should be taken, and high-precision instruments such as a spherical RPA[22] or energy-resolved time-of-flight[25,26] may be useful.

VII. Conclusions

This work experimentally investigated the performance of a passively-fed, ASCENT-fueled porous electrospray thruster with temperature. An MIT iEPS thruster was outfitted with active thermal control and testing was conducted at temperatures from 20°C to 60°C. The thruster's I-V behavior, energy spectra, beam divergence, and mass spectra were captured at various setpoints, and were used to estimate trends in thrust, specific impulse, and efficiency. At higher temperatures the thruster is able to emit higher current at a given voltage, likely due to a decrease in propellant viscosity and/or surface tension. Surprisingly, the thrust was found to remain fairly constant with temperature despite a steeper I-V curve. This is because while the average specific charge of the ion beam decreases with temperature, this is offset by a change in energy efficiency that has not been observed in similar tests with conventional ILs. This study also found that the specific impulse decreases and the thrust-to-power increases with temperature. The results of this work are useful for mission planning for upcoming an technology demonstration, but also hint at interesting emission physics that warrant further study.

Appendix

Table 2: Thruster current-voltage behavior by temperature.

Temp.	**Mode**	**Startup [V]**	**I-V Slope [µA/V]**
20^{o}C	+	942	1.04
	-	-950	-0.99
30^{o}C	+	918	1.26
	-	-918	-1.28
40^{o}C	+	902	1.39
	-	-910	-1.49
50^{o}C	+	894	1.49
	-	-898	-1.79
60^{o}C	+	890	1.50
	-	-894	-1.78

Table 3: Complete performance results, including TOF-inferred and corrected performance.

Temp. [°C]	I_{em} [µA]	V_0 [V]	F_{TOF} [µN]	$I_{sp,TOF}$ [sec]	$F_{TOF}/\mathbb{P}$ [µN/W]	η_p [-]	F [µN]	I_{sp} [sec]	$F/\mathbb{P}$ [µN/W]
20	+150	1160	14.4	817	82.6	0.33	11.7	676	67.3
	+100	1070	8.94	786	83.3	0.33	7.26	658	68.0
	-100	-1060	8.14	804	76.9	0.30	6.88	687	65.1
	-150	-1120	13.2	811	79.0	0.30	11.2	680	66.5
30	+150	1080	14.1	784	86.4	0.33	-	-	-
	+100	1010	9.03	749	88.9	0.33	-	-	-
	-100	-990	7.77	862	79.2	0.32	-	-	-
	-150	-1050	12.5	810	79.2	0.32	-	-	-
40	+150	1020	14.1	756	92.0	0.34	8.48	626	55.4
	+100	980	9.35	738	94.8	0.35	5.63	609	57.1
	-100	-960	7.83	973	82.6	0.37	6.65	843	68.9
	-150	-990	12.5	779	84.4	0.32	10.6	685	71.4
50	+150	1010	16.1	747	108	0.37	-	-	-
	+100	955	10.9	699	114	0.39	-	-	-
	-100	-945	8.45	763	89.3	0.34	-	-	-
	-150	-980	13.0	739	88.5	0.32	-	-	-
60	+150	1010	20.7	663	136	0.46	11.9	582	78.6
	+100	950	12.2	687	128	0.44	7.16	567	73.4
	-100	-945	8.89	738	93.4	0.35	7.01	614	73.8
	-150	-970	13.5	753	93.5	0.34	10.6	641	73.0

Acknowledgments

This work was supported by NASA Space Technology Graduate Research Opportunity (under grant 80NSSC18K1186) and a National Science Foundation Graduate Research Fellowship (under grant 1745302). The authors thank Miles Oglesby for his assistance on thermal circuit construction, and Clark Teems for useful discussions on the expected thermal environments on the GPDM mission. P. C. Lozano thanks the Miguel Alemán-Velasco Foundation for its support.

References

[1]B. J. Colón, M. J. Glaser, E. G. Lightsey, A. R. Bruno, D. P. Cavender, and P. Lozano, "Spectre: Design of a Dual-Mode Green Monopropellant Propulsion System," in *Rocky Mountain AAS GNC*, vol. AAS-094, 2022.

[2]N. J. Williams, A. J. Moore, C. G. Burnside, N. M. Vaughn, S. W. Skinner, L. I. Richard, C. M. Teems, and C. O. Squibb, "Design, Analysis, Testing, and Flight Activities for A Green Propulsion Dual Mode (GPDM) Technology Demonstration Mission," in *JANNAF*, 2024.

[3]A. R. Bruno and P. C. Lozano, "Design and Testing of a Propellant Management System for Bimodal Chemical-Electrospray Propulsion," in *Proceedings of the IEEE Aerospace Conference*, 2021.

[4]A. R. Bruno, M. R. Schroeder, and P. C. Lozano, "Characterization of Electrospray Thrusters with HAN-Based Monopropellants for Multimode Propulsion Applications," in *AIAA SCITECH 2022 Forum*, 2022, p. 2490.

[5]F. J. Higuera, "Model of the meniscus of an ionic-liquid ion source," *Physical Review E*, vol. 77, no. 2, p. 026308, 2008.

[6]M. Gamero-Castano, "Electric-field-induced ion evaporation from dielectric liquid," *Physical review letters*, vol. 89, no. 14, p. 147602, 2002.

[7]X. Gallud and P. C. Lozano, "The emission properties, structure and stability of ionic liquid menisci undergoing electrically assisted ion evaporation," *Journal of Fluid Mechanics*, vol. 933, p. A43, 2022.

[8]P. Lozano and M. Martinez-Sanchez, "Ionic liquid ion sources: Characterization of externally wetted emitters," *Journal of Colloid and Interface Science*, vol. 282, no. 2, pp. 415–421, 2005.

[9]S. Dworski, C. Ma, and C. Ryan, "Effects of Propellant Temperature on Fragmentation in the Plume of a Porous Electrospray Thruster," in *International Electric Propulsion Conference*, Boston, MA & Virtual, Jun. 2022.

[10]M. N. Corrado, "Active Thermal Augmentation and Ultra Dense MEMS-Based Electrospray Thrusters," 2022.

[11]D. Villegas-Prados, J. Cruz, M. Wijnen, S. Correyero, P. Fajardo, and J. Navarro-Cavallé, "Impact of propellant temperature on the emission regime of an externally wetted electrospray system using time-of-flight mass spectrometry," *Acta Astronautica*, vol. 213, pp. 145–155, 2023.

[12]D. Villegas, M. Wijnen, S. Correyero, G. Arboleya, and P. Fajardo, "Impact of the propellant temperature on the performance of externally wetted electrospray thrusters," in *International Electric Propulsion Conference*, Boston, MA & Virtual, Jun. 2022.

[13]R. L. Sackheim and R. K. Masse, "Green Propulsion Advancement: Challenging the Maturity of Monopropellant Hydrazine," *Journal of Propulsion and Power*, vol. 30, no. 2, pp. 265–276, 2014. [Online]. Available: https://doi.org/10.2514/1.B35086

[14]R. Masse, R. A. Spores, S. Kimbrel, M. Allen, E. Lorimor, P. Myers, and C. McLean, "GPIM AF-M315E propulsion system," *51st AIAA/SAE/ASEE Joint Propulsion Conference*, pp. 1–12, 2015, iSBN: 9781624103216.

[15]C. E. Miller, P. C. Lozano, and K. Polzin, "Experimental Measurements of an AF-M315E-fed Ion Electrospray Propulsion System (iEPS)," in *65th JANNAF Propulsion Meeting*, Long Beach, CA, 2018.

[16]J. Macarthur, B. O. Kristinsson, D. Freeman, E. Petro, H. Li, and P. C. Lozano, "Microfluidic and Extractor Electrode Update in the ion-Electrospray Propulsion System," *36th International Electric Propulsion Conference*, pp. 1–8, 2019.

[17]N. Brikner and P. C. Lozano, "The role of upstream distal electrodes in mitigating electrochemical degradation of ionic liquid ion sources," *Applied Physics Letters*, vol. 101, no. 19, pp. 7–10, 2012.

[18]"Supreme 11AOHT-LO Product Information." [Online]. Available: https://www.masterbond.com/tds/supreme-11aoht-lo.

[19]P. C. Lozano, "Energy properties of an EMI-Im ionic liquid ion source," *J. Phys. D: Appl. Phys*, vol. 39, pp. 126–134, 2006.

[20]E. Petro, A. Bruno, P. Lozano, L. Perna, and D. Freeman, "Characterization of the TILE electrospray emitters," in *AIAA Propulsion and Energy 2020 Forum*, 2020.

[21]G. Pettersson, A. Bruno, M. Corrado, B. Medina, and P. Lozano, "Performance Measurement and Propellant Testing for the STEP-1 CubeSat Elecrospray Thrusters," in *International Electric Propulsion Conference*, Boston, MA & Virtual, Jun. 2022.

[22]C. E. Miller, "Characterization of Ion Cluster Fragmentation in Ionic Liquid Ion Sources," Ph.D. dissertation, Massachusetts Institute of Technology, 2019.

[23]*Channeltron Electron Multiplier Handbook for Mass Spectrometry Applications*, Photonis, 2019, available at https://www.photonis.com/system/files/2019-03/Channeltronhandbook.pdf.

[24]M. Gamero-Castano and V. Hruby, "Electrospray as a source of nanoparticles for efficient colloid thrusters," *Journal of Propulsion and Power*, vol. 17, no. 5, pp. 977–987, 2001.

[25]M. Gamero-Castaño and A. Cisquella-Serra, "Electrosprays of highly conducting liquids: A study of droplet and ion emission based on retarding potential and time-of-flight spectrometry," *Physical Review Fluids*, vol. 6, no. 1, p. 013701, 2021.

[26]C. T. Lyne, M. F. Liu, and J. L. Rovey, "A simple retarding-potential time-of-flight mass spectrometer for electrospray propulsion diagnostics," *Journal of Electric Propulsion*, vol. 2, no. 1, p. 13, 2023.